The Plasma Focus- Numerical Experiments Leading Technology

S H Saw[1,2*] and S Lee[1,2,3]

[1]INTI International University, 71800 Nilai, Malaysia
[2] Institute for Plasma Focus Studies, 32 Oakpark Drive, Chadstone, VIC3148, Australia
[3] Nanyang Technological University, National Institute of Education, Singapore 637616
e-mails: sorheoh.saw@newinti.edu.my leesing@optusnet.com.au

*Corresponding author: Prof Dr S H Saw
Mailing Address: INTI International University,
Persiaran Perdana BBN, Putra Nilai, 71800 Nilai, Negeri Sembilan, Malaysia

Tel No: +606 7982031

Short Title: Plasma Focus: Numerical Experiments Lead Technology

Number of:
Pages: 16
Tables: 0
Figures: 4

The Plasma Focus- Numerical Experiments Leading Technology

S H Saw[1,2*] and S Lee[1,2,3]

[1]INTI International University, Nilai, Malaysia
[2]Institute for Plasma Focus Studies, Melbourne, Australia
[3]Nanyang Technological University, National Institute of Education, Singapore

Numerical experiments on the plasma focus have uncovered scaling properties, and are now used routinely to assist design and provide reference points for diagnostics. More importantly guidance has been given regarding the implementation of technology for new generations of constant energy density (per unit mass) plasma focus devices, thus extending the range of scalable plasma focus through seven orders of magnitude of storage energy. Moreover intensive series of experiments have shown that it is a futile expense to reduce static bank inductance L_0 below certain values because of the consistent loading effects of the plasma focus dynamics on the capacitor bank. Thus whilst it was thought that the PF1000 could receive major benefits by reducing L_0, numerical experiments have shown to the contrary that its present L_0 of 30 nH is already optimum and that reducing L_0 would be an expensive fruitless exercise. The numerical experiments also show that the deterioration of the yield scaling law (e.g. the fusion neutron yield scaling with storage energy) is inevitable again due to the consistent loading effect of the plasma focus, which becomes more and more dominant as capacitor bank impedance reduces with increasing capacitance C_0 as storage energy is increased. This line of thinking has led to the suggestion of using higher voltages (as an alternative to increasing C_0) and to seeding of Deuterium with noble gases in order to enhance compression through thermodynamic mechanisms and through radiation cooling effects of strong line radiation. Circuit manipulation e.g. to enhance focus pinch compression by current-stepping is also being numerically experimented upon. Ultimately however systems have to be built, guided by numerical experiments, so that the predicted technology may be proven and realized.

Keywords: Plasma Focus Scaling, Plasma Focus Properties, Plasma Focus Numerical Experiments, Neutron Saturation, New Plasma Focus Devices

1. Introduction

The plasma focus is one of the smaller scale devices which complement the international efforts to build a nuclear fusion reactor [1]. It is an important device for the generation of intense multi-radiation including x-rays, particle beams and fusion neutrons. The physics underlying the mechanisms for the generation of these radiations in the plasma focus is still not completely known although there have been intensive investigations for the past five decades. Experimental and theoretical work on the focus has reached quite high levels. For example, detailed simulation work on the plasma focus had been carried out since 1971 [2] and by 1998 a large range of devices has been constructed from 1 kJ small focus to hundreds of kJ large focus [3]. Advanced experiments have been carried out on the dynamics, radiation, instabilities and non-linear phenomena [3]. Yet despite all these intensive studies, very little regarding scaling appears to be documented with the exception of the scaling law for neutron yield. More recent work, mainly numerical experiments, has thrown much needed light on other aspects of scaling such as how the dimensions of the dense focused plasma (the focus pinch) and the pinch lifetime scale with apparatus dimensions, the dominating dimension being the anode radius [4]. Another important finding is that the energy density per unit mass remains a constant throughout the range of neutron-optimized plasma focus [4]. In this regard the rules-of-thumb scaling properties for neutron-optimized plasma focus devices operating in deuterium are listed below:

Axial phase energy density (per unit mass)	constant
Radial phase energy density (per unit mass)	constant
Pinch radius ratio	constant
Pinch length ratio	constant
Pinch duration per unit anode radius	constant

These rules-of-thumb summarize the results from intensive numerical experiments. The dense hot plasma pinch of a small E_0 plasma focus and that of a big E_0 plasma focus have essentially the same energy density per unit mass. The big E_0 plasma focus has a bigger physical size and a bigger discharge current. The size of the plasma pinch scales proportionately to the current and to the anode radius, as does the duration of the plasma pinch. The bigger E_0, the bigger I_{peak}, the bigger 'a' has to be, hence the larger the plasma pinch and the longer the duration of the plasma pinch. The larger size and longer duration of the big E_0 plasma pinch are essentially the properties leading to the bigger neutron yield compared to the yield of the small E_0 plasma focus.

We may note that the speeds and also the plasma temperature T_{pinch} are all measures of the energy per unit mass. As an example comparing the Chilean PF-400J [5] with the 1 MJ PF1000 [6], the numerical experiments show quite remarkably that the energy density at the focus pinch varies so little (factor of 5) over a range of device energy of more than 3 orders of magnitude (factor >1000) with a neutron yield difference of 5 orders of magnitude computed from numerical experiments and verified by actual measurements on the device.

The important observation by Lee and Serban (1996) of constancy in energy density was instrumental in the extension of the range of constant energy density scalable plasma focus devices to a remarkable 10^7, with the development of the 0.1 J Nanofocus by Soto 2009 [7]. This is the first example of numerical experiments guiding technology. Conversely once the Nanofocus was successfully developed, its operation confirmed that even at 0.1 J the plasma focus still demonstrated the same constancy of energy density per unit mass.

This paper proceeds to discuss other important examples of numerical experiments leading technology in the development of plasma focus devices.

2. Introduction to the Lee model code

The Lee model code couples the electrical circuit with plasma focus dynamics, thermodynamics, and radiation, enabling a realistic simulation of all gross focus properties. The basic model, described in 1984 [8], was successfully used to assist several projects [4,9-11]. Radiation-coupled dynamics was included in the five-phase code, leading to numerical experiments on radiation cooling [12]. The vital role of a finite small disturbance speed discussed by Potter in a *Z*-pinch situation [13] was incorporated together with real gas thermodynamics and radiation-yield terms. This version of the code assisted other research projects [14-19] and was web published in 2000 [20] and 2005 [21]. Plasma self-absorption was included in 2007 [20], improving the SXR yield simulation. The code has been used extensively in several machines including UNU/ICTP PFF [11,12,14,16-19], NX2 [15,17,22,23], and NX1 [23,24] and has been adapted for the Filippov-type plasma focus DENA [25]. A recent development is the inclusion of the neutron yield Y_n using a beam–target mechanism [26-30], incorporated in recent versions [31,32] of the code (versions later than RADPFV5.13), resulting in realistic Y_n scaling with I_{pinch} [33-37]. The versatility and utility of the model are demonstrated in its clear distinction of I_{pinch} from I_{peak} [28] and the recent uncovering of a plasma focus pinch current limitation effect [29,30], as static inductance is reduced towards zero. Extensive numerical experiments had been carried out systematically resulting in the uncovering of neutron [26,27,36] and SXR [38-44] scaling laws over a wider range of energies and currents than attempted before. The numerical experiments also gave insight into the nature and cause of 'neutron saturation [27,34,36,44]. The description, theory, code, and a broad range of results of this "Universal Plasma Focus Laboratory Facility" are available for download from [32].

A brief description of the 5-phase model is given in the following.

2.1 The 5-phases

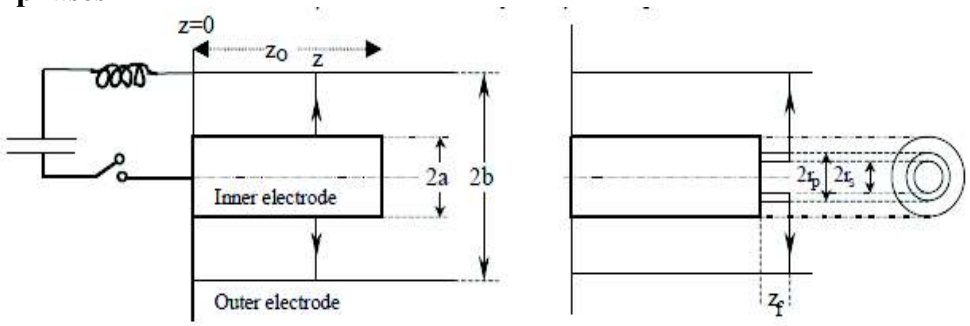

Figure 1. Schematic of the axial and radial phases. The left section depicts the axial phase, the right section the radial phase. In the left section, z is the effective position of the current sheath-shock front structure. In the right section r_s is the position of the inward moving shock front driven by the piston at position r_p. Between r_s and r_p is the radially imploding slug, elongating with a length z_f. The capacitor, static inductance and switch powering the plasma focus is shown for the axial phase schematic only.

The five phases (*a-e*) are summarised [28,31-35,38, 42-44] as follows:
a. Axial Phase (see Figure 1 left part): Described by a snowplow model with an equation of motion which is coupled to a circuit equation. The equation of motion incorporates the axial

phase model parameters: mass and current factors f_m and f_c. The mass swept-up factor [45,46] f_m accounts for not only the porosity of the current sheet but also for the inclination of the moving current sheet-shock front structure, boundary layer effects, and all other unspecified effects which have effects equivalent to increasing or reducing the amount of mass in the moving structure, during the axial phase. The current factor f_c accounts for the fraction of current effectively flowing in the moving structure (due to all effects such as current shedding at or near the back-wall, and current sheet inclination).

b. Radial Inward Shock Phase

Described by 4 coupled equations using an elongating slug model. The first equation computes the radial inward shock speed from the driving magnetic pressure. The second computes the axial column elongation speed. The third computes the speed of the current sheath (magnetic piston), allowing the sheath to separate from the shock front by applying an adiabatic approximation [16]. The fourth is the circuit equation. Thermodynamic effects due to ionization and excitation are incorporated into these equations, these effects being particularly important for gases other than hydrogen and deuterium. Temperature and number densities are computed using shock-jump equations. A communication delay between shock front and current sheath due to the finite small disturbance speed [13,32] is implemented. The model parameters, radial phase mass swept-up and current factors f_{mr} and f_{cr} are incorporated in all three radial phases.

c. Radial Reflected Shock (RS) Phase: When the shock front hits the axis, because the plasma is collisional, a reflected shock develops which moves radially outwards, whilst the radial current sheath continues to move inwards. Four coupled equations are also used, these being for the reflected shock moving radially outwards, the piston moving radially inwards, the elongation of the annular column and the circuit. The plasma temperature behind the reflected shock undergoes a jump by a factor of 2. Number densities are computed using reflected shock jump equations.

d. Slow Compression (Quiescent) or Pinch Phase: When the out-going reflected shock hits the inward moving piston, the compression enters a radiative phase. For gases such as neon, radiation emission may enhance the compression as energy loss/gain terms from Joule heating and radiation are included in the piston equation of motion. Three coupled equations are used; these being for piston radial motion, pinch column elongation and for the circuit. The duration of this slow compression phase is set as the time of transit of small disturbances across the pinched plasma column. The computation of this phase is terminated at the end of this duration.

e. Expanded Column Axial Phase: To simulate the current trace beyond this point we allow the column to suddenly attain the radius of the anode, and use the expanded column inductance for further integration. In this final phase the snow plow model is used, and two coupled equations are used similar to the axial phase above. This phase is not considered important as it occurs after the focus pinch.

We note [38,42,43] that in radial phases *b, c* and *d*, axial acceleration and ejection of mass caused by necking curvatures of the pinching current sheath result in time-dependent strongly center-peaked density distributions. Moreover the transition from phase *d* to phase *e* is observed in laboratory measurements to occur in an extremely short time with plasma/current disruptions resulting in localized regions of high densities and temperatures [47]. These centre-peaking density effects and localized regions are not modeled in the code, which consequently computes only an average uniform density and an average uniform temperature which are considerably lower than measured peak density and temperature. However, because the four model parameters are obtained by fitting the computed total current waveform to the measured total current waveform, the model incorporates the energy and mass balances equivalent, at least in the gross sense, to all the processes which are not even

specifically modeled. Hence the computed gross features such as speeds and trajectories and integrated soft x-ray yields have been extensively tested in numerical experiments for several machines and are found to be comparable with measured values.

2.2 The model code as a general diagnostic tool

The model code now includes a sheet in which is displayed charts of the properties of the particular shot including: total discharge current and plasma current, tube voltage, axial trajectories and speeds, tube inductance and total inductive energy, piston work and Joule work related to the dynamic resistance, the dynamic resistance, ion and electron number density (spatial uniform averaged and peak) , plasma temperature (spatial uniform averaged and peak), computed soft x-ray power; all these properties are displayed as functions of time, in the axial phase (where applicable) and in the radial phase. The model code provides information to guide experimental measurements and can be considered as a powerful diagnostics tool as well [34].

3. Further examples of numerical experiments leading technology

Moreover, using such simulation, series of experiments have been systematically carried out to look for behaviour patterns of the plasma focus. Insights uncovered by the series of experiments include: (i) pinch current limitation effect as static inductance is reduced; (ii) neutron and SXR scaling laws; (iii) a global scaling law for neutrons versus storage energy combining experimental and numerical experimental data; and (iv) insight into the nature and a fundamental cause of neutron saturation. These are significant achievements in which numerical experiments lead technology either in uncovering important new effects or in extending the range of scaling laws beyond that which could be accomplished by machines, hence requiring the re-interpretation of the extended scaling laws.

3.1. Insight 1-Pinch Current Limitation Effect as Static Inductance is Reduced Towards Zero

In a recent paper [6] there was expectation that the MJ plasma focus PF1000 could increase its discharge and pinch currents, and consequently neutron yield by a reduction of its external or static inductance L_0. To investigate this point, experiments were carried out using the Lee Model code. Unexpectedly, the results indicated that whilst I_{peak} indeed progressively increased with reduction in L_0, no improvement may be achieved due to a pinch current limitation effect [29,30]. Given a fixed C_0 powering a plasma focus, there exists an optimum L_0 for maximum I_{pinch}. Reducing L_0 further will increase neither I_{pinch} nor Y_n. The numerical experiments leading to this unexpected result is described below.
A measured current trace of the PF1000 with C_0 = 1332 μF, operated at 27 kV, 3.5 torr deuterium, has been published [6], with cathode/anode radii b = 16 cm, a = 11.55 cm and anode length z_0 = 60 cm. In the numerical experiments we fitted external (or static) inductance L_0= 33.5 nH and stray resistance r_0 = 6.1 mΩ (damping factor $RESF= r_0/(L_0/C_0)^{0.5}$ = 1.22). The fitted model parameters are: f_m = 0.13, f_c = 0.7, f_{mr} = 0.35 and f_{cr}= 0.65. The computed current trace [26-29] agrees very well with the measured trace through all the phases, axial and radial, right down to the bottom of the current dip indicating the end of the pinch phase as shown in Figure.2.

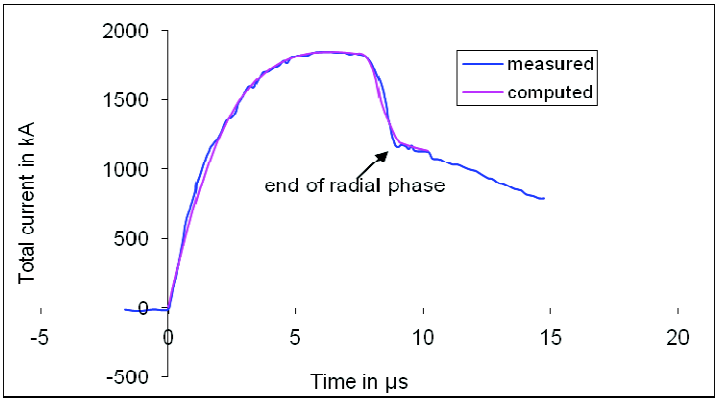

Figure 2. Fitting computed current to measured current traces to obtain fitted parameters f_m = 0.13, f_c = 0.7, f_{mr} = 0.35 and f_{cr}= 0.65. The measured current trace was for the PF1000 at 27 kV, storage capacity of 1332 µF and fitted static inductance of 33.5 µH.

We carried out numerical experiments for PF1000 using the machine and model parameters determined from Figure 2. Operating the PF1000 at 35 kV and 3.5 torr, we varied the anode radius a with corresponding adjustment to b to maintain a constant c=b/a=1.39 and in order to keep the peak axial speed at 10 cm/µs. The anode length z_0 was also adjusted to maximize I_{pinch} as L_0 was decreased from 100 nH progressively to 5 nH.
As expected, I_{peak} increased progressively from 1.66 to 4.4 MA. As L_0 was reduced from 100 to 35 nH, I_{pinch} also increased, from 0.96 to 1.05 MA. However, then unexpectedly, on further reduction from 35 to 5 nH, I_{pinch} stopped increasing, instead decreasing slightly to 1.03 MA at 20 nH, to 1.0 MA at 10 nH, and to 0.97 MA at 5 nH. Y_n also had a peak value of $3.2\text{x}10^{11}$ at 35 nH.
This effect was explained by examining the energy distribution in the system at the end of the axial phase (see Figure 2) just before the current drops from peak value I_{peak} and then again near the bottom of the almost linear drop to the pinch phase indicated by the arrow pointing to 'end of radial phase'. The pinch current limitation was shown to be a combination of the two complex effects, namely, the energy distribution resulting from the interplay of the various inductances involved in the plasma focus processes abetted by the increasing coupling of C_o to the inductive energetic processes, as L_0 is reduced.
From the pinch current limitation effect, it is clear that given a fixed C_0 powering a plasma focus, there exists an optimum L_0 for peak I_{pinch}. Reducing L_0 further will increase neither I_{pinch} nor Y_n.

3.2. Insight 2-Scaling Laws for Neutron

The neutron yield is computed using a phenomenological beam-target neutron generating mechanism described recently by Gribkov et al [6] and adapted to yield the following equation. A beam of fast deuteron ions is produced by diode action in a thin layer close to the anode, with plasma disruptions generating the necessary high voltages. The beam interacts with the hot dense plasma of the focus pinch column to produce the fusion neutrons. The beam-target yield is derived [14,16, 35-39] as:

$$Y_{b\text{-}t} = C_n\, n_i\, I_{pinch}^{\,2} z_p^{\,2} (\ln (b/r_p))\sigma / U^{0.5} \qquad (1)$$

where n_i is the ion density, b is the cathode radius, r_p is the radius of the plasma pinch with length z_p, σ the cross-section of the D-D fusion reaction, n- branch [48] and U, the beam

energy. C_n is treated as a calibration constant combining various constants in the derivation process.
The D-D cross-section is sensitive to the beam energy in the range 15-150 kV; so it is necessary to use the appropriate range of beam energy to compute σ. The code computes induced voltages (due to current motion inductive effects) V_{max} of the order of only 15-50 kV. However it is known, from experiments that the ion energy responsible for the beam-target neutrons is in the range 50-150 keV [3,6], and for smaller lower-voltage machines the relevant energy could be lower at 30-60 keV [19]. Thus in line with experimental observations the D-D cross section σ is reasonably obtained by using $U = 3V_{max}$. This fit was tested by using U equal to various multiples of V_{max}. A reasonably good fit of the computed neutron yields to the measured published neutron yields at energy levels from sub-kJ to near MJ was obtained when the multiple of 3 was used; with poor agreement for most of the data points when for example a multiple of 1 or 2 or 4 or 5 was used. The model uses a value of C_n=2.7x10^7 obtained by calibrating the yield [26,27,29], at an experimental point of 0.5 MA.
The thermonuclear component is also computed in every case and it is found that this component is negligible when compared with the beam-target component.

3.2.1. Scaling laws for neutrons from numerical experiments over a range of energies from 10kJ to 25 MJ

We apply the Lee model code to the MJ machine PF1000 over a range of C_0 to study the neutrons emitted by PF1000-like bank energies from 10kJ to 25 MJ.
As shown earlier the PF1000 current trace has been used to fit the model parameters, with very good fitting achieved between the computed and measured current traces (Figure 2). With no measured current waveforms available for the higher megajoule numerical experiments, it is reasonable to keep the model parameters that we have got from the PF1000 fitting.
The optimum pressure for this series of numerical experiments is 10 torr and the ratio $c=b/a$ is retained at 1.39. For each C_0, anode length z_0 is varied to find the optimum. For each z_0, anode radius a_0 is varied so that the end axial speed is 10 cm/μs. The numerical experiments were carried out for C_0 from 14 μF to 39960 μF corresponding to energies from 8.5 kJ to 24.5 MJ [27].
Over wide ranges of energy, optimizing pressure, anode length and radius, the scaling laws for Y_n [26,27,33,35] obtained through numerical experiments are listed here:

Y_n=3.2x10^{11} $I_{pinch}^{4.5}$
Y_n=1.8x10^{10} $I_{peak}^{3.8}$ I_{peak} (0.3 to 5.7), I_{pinch} (0.2 to 2.4) in MA.
$Y_n \sim E_0^{2.0}$ at tens of kJ to
$Y_n \sim E_0^{0.84}$ at MJ level (up to 25MJ)

Note that Y_n starts at a scaling index of 2.0 at low energies but deteriorates to a scaling index of 0.84 at high energies. This deterioration has great significance and will be discussed later.
These laws extend the range beyond presently available machines and lend further credence to the generality of scaling properties and scaling laws already indicated by the observation of constant energy density. They thus provide useful references for design considerations of new plasma focus machines beyond presently experienced regimes, particularly if they are intended to operate as optimized neutron sources. Thus the development of these general scaling laws is another example of numerical experiments leading and guiding technology.

3.3 Insight 3-Scaling Laws for Soft X-ray Yield

In the code [14,16,44], neon line radiation Q_L is calculated as follows:

$$\frac{dQ_L}{dt} = -4.6x10^{-31} n_i^{\,2} Z Z_n^{\,4} \left(\pi r_p^{\,2}\right) z_f / T \qquad (2)$$

where for the temperatures of our interest we take the SXR yield $Y_{sxr} = Q_L$. Z_n is atomic number.

Hence the SXR energy generated within the plasma pinch depends on the properties: number density n_i, effective charge number Z, pinch radius r_p, pinch length z_f and T. It also depends on the pinch duration since in our code Q_L is obtained by integrating over the pinch duration. This generated energy is then reduced by the plasma self-absorption which depends primarily on density and temperature; the reduced quantity of energy is then emitted as the SXR yield. These effects are included in the modelling by computing volumetric plasma self-absorption factor A derived from the photonic excitation number M which is a function of Z_n, n_i, Z and T. However, in our range of operation, the numerical experiments show that the self absorption is not significant. It was first pointed out by Liu Mahe [14,17] that a temperature around 300 eV is optimum for SXR production. Shan Bing's subsequent work [15] and our experience through numerical experiments suggest that around $2x10^6$ K (below 200 eV) or even a little lower could be better. Hence unlike the case of neutron scaling, for SXR scaling there is an optimum small range of temperatures (T windows) to operate.

3.3.1 Scaling laws for neon SXR over a range of energies from 0.2 kJ to 1 MJ

We use the Lee model code to carry out a series of numerical experiments over the energy range 0.2 kJ to 1 MJ [38]. The following parameters are kept constant : (i) the ratio $c=b/a$ (kept at 1.5, which is practically optimum according to our preliminary numerical trials; (ii) the operating voltage V_0 (kept at 20 kV); (iii) static inductance L_0 (kept at 30 nH, which is already low enough to reach the I_{pinch} limitation regime [29,30] over most of the range of E_0 we are covering) and; (iv) the ratio of stray resistance to surge impedance $RESF$ (kept at 0.1, representing a highperformance modern capacitor bank). The model parameters [46] f_m, f_c, f_{mr}, f_{cr} are also kept at fixed values 0.06, 0.7, 0.16 and 0.7, representing average values from the range of machines that we have studied. A typical example of a current trace for these parameters is shown in Figure 3.

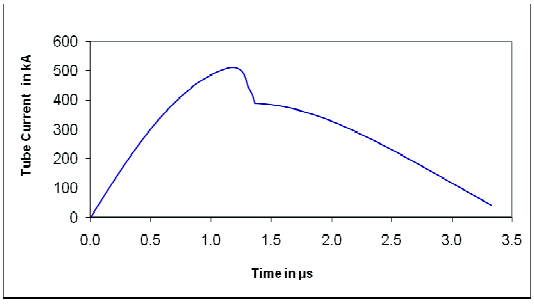

Figure 3. Computed total curent versus time for L_0= 30 nH and V_0= 20 kV, C_0= 30 µF, $RESF$ = 0.1, c = 1.5 and model parameters f_m, f_c, f_{mr}, f_{cr} are fixed at 0.06, 0.7, 0.16 and 0.7 for optimised a = 2.285 cm and z_0 = 5.2 cm.

The storage energy E_0 is varied by changing the capacitance C_0. Parameters that are varied are operating pressure P_0, anode length z_0 and anode radius a. Parametric variation at each E_0 follows the order; P_0, z_0 and a until all realistic combinations of P_0, z_0 and a are investigated.

At each E_0, a P_0 is fixed, a z_0 is chosen and a is varied until the largest Y_{sxr} is found. Then keeping the same values of E_0 and P_0, another z_0 is chosen and a is varied until the largest Y_{sxr} is found. This procedure is repeated until for that E_0 and P_0, the optimum combination of z_0 and a is found. Then keeping the same value of E_0, another P_0 is selected. This procedure is repeated until for a fixed value of E_0, the optimum combination of P_0, z_0 and a is found.
The procedure is then repeated with a new value of E_0. In this manner after systematically and extensive numerical experiments over wide ranges of energy, optimizing pressure, anode length and radius, the scaling laws for neon SXR are found to be [38]:

$Y_{sxr}=8.3\text{x}10^3\text{x}I_{pinch}^{3.6}$
$Y_{sxr}=600\text{x}I_{peak}^{3.2}$; I_{peak} (0.1 to 2.4), I_{pinch} (0.07 to1.3) in MA.
$Y_{sxr}\sim E_0^{1.6}$ (kJ range)
$Y_{sxr}\sim E_0^{0.8}$ (towards MJ).

We stress that these scaling laws for neon SXR are developed through numerical experiments.
Only scant reliable measured SXR data [49] is available to provide any but the most rudimentary scaling. Hence these scaling laws for neon SXR provide useful references and facilitate the understanding of present plasma focus machines. More importantly, these scaling laws are also useful for design considerations of new plasma focus machines particularly if they are intended to operate as neon SXR sources. The Lee Model code which already incorporates the thermodynamic data for other gases including N, Kr, Xe can readily be run to provide similar scaling laws for the other gases.

3.4. Insight 4- Neutron Saturation

It was observed early in plasma focus research [3,50] that neutron yield $Y_n\sim E_0^2$ where E_0 is the capacitor storage energy. Such scaling gave hopes of possible development as a fusion energy source. Devices were scaled up to higher E_0. It was then observed that the scaling deteriorated, with Y_n not increasing as much as suggested by the E_0^2 scaling. In fact some experiments were interpreted as evidence of a neutron saturation effect [3] as E_0 approached several hundreds of kJ. As recently as 2006 Krauz [51] and November 2007, Scholz [52] have questioned whether the neutron saturation was due to a fundamental cause or to avoidable machine effects such as incorrect formation of plasma current sheath arising from impurities or sheath instabilities. We should note here that the region of discussion (several hundreds of kJ approaching the MJ region) is in contrast to the much higher energy region discussed by Schmidt at which there might be expected to be a decrease in the role of beam target fusion processes [3].

3.4.1. The global neutron scaling law

The neutron scaling laws described above in section 3.2.1 also showed that whereas at energies up to tens of kJ the $Y_n\sim E_0^2$ scaling held, deterioration of this scaling became apparent above the low hundreds of kJ. This deteriorating trend worsened and tended towards $Y_n\sim E_0^{0.8}$ at tens of MJ. The results of these numerical experiments are summarized in Figure. 4 with the solid line representing results from numerical experiments. Experimental results from 0.4 kJ to MJ, compiled from several available published sources [3-7,26,53,54], are also included as squares in the same figure. The combined experimental and numerical experimental results [36] (see Figure 4) appear to have general agreement particularly with regards to the $Y_n\sim E_0^2$ at energies up to 100 kJ, and the deterioration of the scaling from low

hundreds of kJ to the 1 MJ level. The global data of Figure. 1 suggests that the apparently observed neutron saturation effect is overall not in significant variance with the deterioration of the scaling shown by the numerical experiments. We note that the compilation of this global neutron scaling law is not possible without the input of extensive numerical experiments since the measured data are too patchy and obviously influenced by effects contributed by disparate design of various machines. Hence only the rigours of extensive numerical experiments can provide firm guidance showing a clear scaling trend into which the experimental data may be seen to fall. Thus the derivation of this global neutron scaling is another example of numerical experiments guiding and leading technology.

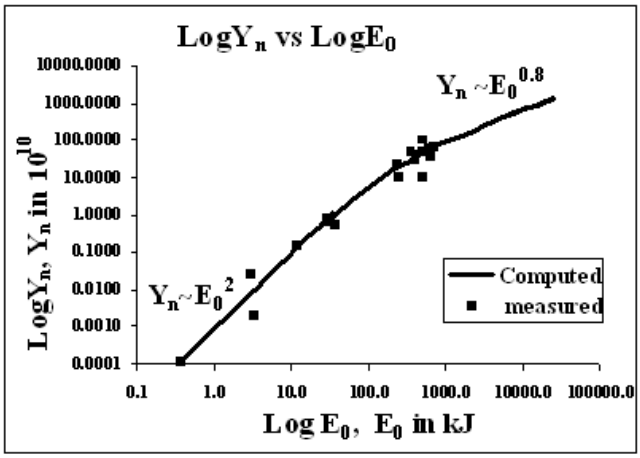

Figure 4. The global scaling law, combining experimental and numerical data. The global data illustrates Y_n scaling observed in numerical experiments from 0.4 kJ to 25 MJ (solid line) using the Lee model code, compared to measurements compiled from publications (squares) of various machines from 0.4 kJ to 1 MJ.

3.4.2. The dynamic resistance- explaining the deterioration of neutron scaling

A simple yet compelling analysis of the cause of this neutron saturation has been published [36]. Associated with any time-varying inductance dL/dt there is fundamentally a resistance of magnitude (1/2) dL/dt due to the motion associated with *dL/dt* ; which we call the dynamic resistance DR. Note that this is a general result and is independent of the actual processes involved. In the case of the plasma focus axial phase, the motion of the current sheet imparts power to the shock wave structure with consequential shock heating, Joule heating, ionization, radiation etc. The total power imparted at any instant is just the amount $(½)(dL/dt)I^2$, with this amount powering all consequential processes.

The time varying tube inductance is $L=(\mu/2\pi)ln(c)\ z$, where $c=b/a$ and μ is the permeability of free space. $dL/dt=2x10^{-7}(lnc)\ dz/dt$ in SI units. Typically on switching, as the capacitor discharges, the current rises towards its peak value, the current sheet is accelerated, quickly reaching nearly its peak speed and continues accelerating slightly towards its peak speed at the end of the axial phase. Thus for most of its axial distance the current sheet is travelling at a speed close to the end-axial speed. For neutron optimized operation in deuterium the end-axial speed is observed to be about 10 cm/μs over the whole range of devices [4]. As shown earlier this is related to the constancy of energy density. This fixes *dL/dt* as $1.4x10^{-2}$H/s (14 mΩ) for all the devices, if we take the radius ratio $c=b/a=2$. This value of *dL/dt* changes by at most a factor of 3, taking into account the variation of *c* from low values of 1.4 (generally for larger machines) to 4 (generally for smaller machines). Thus over the range of devices

there is a constant dynamic resistance of 7 mΩ, associated with the current sheet motion during the axial phase. We also note that for an optimized machine the radial phase has to occur at around or just after the peak of the discharge current. This means that the peak discharge current is determined by the axial phase.

We now resolve the problem into its most basic form as follows. We have a generator (the capacitor bank charged to say V_0=30 kV), with an impedance of $Z_0=(L_0/C_0)^{0.5}$ driving a load with a near constant resistance of 7 mΩ. The bank static inductance L_0 in high-performance machines has a typical value of 30 nH. Thus at low C_0=1μF (0.45 kJ) we have Z_0=173 mΩ driving 7 mΩ; whilst at high C_0=10000 uF (4.5MJ) we have Z_0=1.7 mΩ driving 7 mΩ. Thus at low C_0 (low E_0) the circuit is dominated by Z_0 and increasing the value of E_0 (C_0) lowers the value of Z_0 thus increasing Ipeak~V_0/ Z_0 by factor approximately $C_0^{0.5}$ or $E_0^{0.5}$. Thus at low E_0 of say 1 kJ, increasing the energy 9 times, increase I_{peak} by approx 3 times. On the other hand at high energies of 1 MJ, increasing E_0 by a factor of 9 times, increases I_{peak} by a factor of less than 1.3. At very high energies the circuit is completely dominated by the constant dynamic resistance and increasing E_0 any further will not increase I_{peak} at all.
Summarising at low energies $I_{peak} \sim C_0^{0.5}$ whilst at high energies I_{peak} tends to an asymptotic value of V_0/7 mΩ~4.3 MA.
Thus the apparently observed neutron 'saturation' which is more accurately represented as a neutron scaling deterioration is inevitable because of the dynamic resistance. In line with current plasma focus terminology we will continue to refer to this scaling deterioration as 'saturation'. The above analysis applies to the Mather-type plasma focus. The Filippov-type plasma focus does not have a clearly defined axial phase. Instead it has a lift-off phase and an extended pre-pinch radial phase which determine the value of I_{peak}. During these phases the inductance of the Filippov discharge is changing, and the changing $L(t)$ will develop a dynamic resistance which will also have the same current 'saturation' effect as the Filippov bank capacitance becomes big enough.

The same scaling deterioration is also observed in the yield of Neon SXR (see yield equations above for kJ and MJ ranges) and we expect for other radiation yields as well. The speed restrictions for a plasma focus operating in neon is not the same as that in deuterium. Nevertheless there is a speed window related to the optimum temperature window. This again requires fixing the dynamic resistance of the axial phase for the neon plasma focus within certain limits typically the dynamic resistance equivalent to an axial speed range of 5-8 cm per microsecond. This dynamic resistance and its interaction with the capacitor bank impedance as storage energy is increased is again the cause of the scaling deterioration.

4. Beyond presently observed neutron saturation regimes

Moreover the 'saturation' as observed in presently available data is due also to the fact that all tabulated machines operate in a narrow range of voltages of 15-50 kV. Only the SPEED machines, most notably SPEED II [55] operated at low hundreds of kV. No extensive data have been published from the SPEED machines. Moreover SPEED II, using Marx technology, has a large bank surge impedance of 50 mΩ which itself would limit the current. If we operate a range of such high voltage machines at a fixed high voltage, say 300 kV, with ever larger E_0 until the surge impedance becomes negligible due to the very large value of C_0. then the 'saturation' effect would still be there, but the level of 'saturation' would be proportional to the voltage. In this way we can go far above presently observed levels of neutron 'saturation'; moving the research, as it were into presently beyond-saturation regimes.

Could the technology be extended to 1MV? That would raise I_{peak} to beyond 15 MA and I_{pinch} to over 6 MA. Also multiple Blumleins at 1 MV, in parallel, could provide driver impedance of 100 mΩ, matching the radial phase dynamic resistance and provide fast rise currents peaking at 10 MA with I_{pinch} value of perhaps 5 MA. Bank energy would be several MJ. The push to higher currents may be combined with proven neutron yield enhancing methods such as doping deuterium with low % of krypton [56]. Further increase in pinch current might be by fast current injection near the start of the radial phase. This could be achieved with charged particle beams or by circuit manipulation such as current-stepping [57, 58]. The Lee model is ideally suited for testing circuit manipulation schemes.

5. Conclusions

This paper has reviewed the progress made in numerical experiments which have established guidelines for technological applications. Scaling parameters have been established the most important being the constancy of energy density per unit mass in both the axial and radial phases during the dynamic phases as well as the final hot pinch phase. This understanding from numerical experiments has been instrumental to the development of the Nanofocus which has extended the range of scalable constant energy density plasma focus devices over a remarkable 7 orders of magnitude in storage energy from 0.1 J to 1 MJ. The numerical experiments have uncovered a current and neutron yield limitation effect as circuit inductance is lowered; thus pointing out the expensive futility of trying to achieve near zero inductances. The numerical experiments have led to comprehensive scaling laws in neutron and neon SXR yields opening a clear way for radiation yields from other gases. The numerical experiments have also formed the guidance for combined data to fall into a global scaling law for neutron yield as a function of storage energy. Moreover the scaling deterioration and eventual 'saturation' of circuit current are ascribed to the energy density constancy manifested in the form of a constancy in dynamic resistance of the axial phase.
The understanding of this situation points to a new class of plasma focus devices to overcome the 'saturation' of the electric current. One way is for plasma focus technology to move to ultra high voltage technology and take advantage of circuit manipulation techniques [31, 38, 44, 49-51] in order to move into a new era of high performance. Numerical experiments are also underway to quantify the effect of radiation cooling and collapse on the enhancement of radiation yield with the aim of further guiding the development of doped deuterium for neutron enhancement. Thus in many ways numerical experiments are pointing the way to technology. Ultimately however systems have to be built, guided by numerical experiments, so that the predicted technology may be proven and realized.

References

1. Lee S. (2009). Nuclear fusion and the Plasma Focus. Tubav Conferences Nuclear & Renewable Energy Sources Procs:pg 9-18.
2. D E Potter. (1971). Numerical Studies of the Plasma Focus. Phys. Fluids, **14**, 1911-1914 .
3. Bernard A., Bruzzone H., Choi P., Chuaqui H., Gribkov V., Herrera J., Hirano K., Krejci A., Lee S., Luo C., Mezzetti F., Sadowski M., Schmidt, H., Ware, K., Wong, C.S., Zoita, V. (1998). Scientific Status of Plasma focus Research. *Moscow J Physical Society,* **8***,* 93-170.
4. Lee S. and Serban A. (1996). Dimensions and lifetime of the plasma focus pinch. *IEEE Trans. Plasma Sci.*, 1996**,** ***24***, no. 3, 1101–1105.
5. Soto, L. (2005). New trends and future perspectives on plasma focus research *Plasma Phys. Control. Fusion*, **47** A361.
6. Gribkov V. A., Banaszak A., Bienkowska B., Dubrovsky A. V, Ivanova-Stanik I., Jakubowski L., Karpinski L., Miklaszewski R. A., Paduch M., Sadowski M. J., Scholz M., Szydlowski A., and Tomaszewski K.(2007). Plasma dynamics in the PF-1000 device under fullscale energy storage: II. Fast electron and ion characteristics versus neutron emission parameters and gun optimization perspectives, *J. Phys. D,Appl. Phys.*, ***40*****,** , pp. 3592–3607.
7. Soto, L, Pavez C, Moreno J, Barbaglia, M and Clausse, A.(2009). Nanofocus: an ultra-miniature dense pinch plasma focus device with submillimetric anode operating at 0.1 J, Plasma Sources Sci. Technol. 18 015007 (5pp).
8. Lee, S. (1984). Plasma focus model yielding trajectory and structure. In *Radiations in Plasmas*, McNamara, B., Ed.; World Scientific, Singapore: Volume **II**, pp. 978–987.
9. Tou, T. Y.; Lee, S.; Kwek, K. H. (1989). Non perturbing plasma focus measurements in the run-down phase. *IEEE Trans. Plasma Sci.*, **17**, no. 2, 311–315.
10. Lee, S. (1991). A sequential plasma focus. *IEEE Trans. Plasma Sci.*, ***19***, no.5,
11. Lee, S.; Tou, T. Y.; Moo, S. P.; Eissa, M. A.; Gholap, A. V.; Kwek, K. H.; Mulyodrono, S.; Smith, A. J.; Suryadi, S.; Usada, W.;. Zakaullah, M. (1988). A simple facility for the teaching of plasma dynamics and plasma nuclear fusion. *Amer. J. Phys.*, ***56****,* no. 1, 62–68.
12. Jalil bin Ali. (1990). *Development and studies of a small plasma focus*, Ph.D. Dissertation; Universiti Teknologi Malaysia.
13. Potter, D. E. (1978). The formation of high-density z-pinches. *Nucl. Fusion.* ***18***, 813–823.
14. Liu M. (2006). Soft X-rays from compact plasma focus, Ph.D. dissertation, NIE, Nanyang Technological Univ., Singapore, 2006. ICTP Open Access Archive. [Online]. Available: http://eprints.ictp.it/327/
15. Bing S. (2000). Plasma dynamics and X-ray emission of the plasma focus, Ph.D. dissertation, NIE, Nanyang Technological Univ., Singapore. ICTP Open Access Archive. [Online].: http://eprints.ictp.it/99/
16. Serban A. and Lee S. (1998). Experiments on speed-enhanced neutron yield from a small plasma focus, *J. Plasma Phys.*, ***60***, no. 1, pt. 1, pp. 3–15.
17. Liu M.H., Feng X.P., S. V. Springham, and Lee S. (1998). Soft X-ray measurement in a small plasma focus operated in neon, *IEEE Trans. Plasma Sci.*, ***26***, no. 2, pp. 135–140.
18. Lee S. (1998). In *Twelve Years of UNU/ICTP PFF—A Review*. Trieste, Italy: Abdus Salam ICTP, pp. 5–34. IC/ 98/ 231, ICTP Open Access Archive. [Online]. Available: http://eprints.ictp.it/31/
19. Springham S. V., Lee S., and Rafique M. S.(2000). Correlated deuteron energy spectra and neutron yield for a 3 kJ plasma focus, *Plasma Phys. Control. Fusion*, **42***,* no. 10, pp. 1023–1032.
20. Lee S. (2010). [Online]. Available: http://ckplee.myplace.nie.edu.sg/plasmaphysics/
21. Lee S. (2005). *ICTP Open Access Archive*, 2005. [Online]. Available: http://eprints.ictp.it/85/
22. Wong D., Lee P., Zhang T., Patran A., Tan T. L., Rawat R. S., and Lee S.(2007). An improved radiative plasma focus model calibrated for neonfilled NX2 using a tapered anode, *Plasma Sources Sci. Technol*. ***16***, no. 1, pp. 116–123.
23. Lee S., P. Lee, Zhang G., Feng X., Gribkov V. A., Liu M., Serban A., and Wong T. (1998). High rep rate high performance plasma focus as a powerful radiation source, *IEEE Trans. Plasma Sci.*, ***26***, no. 4, pp. 1119–1126.

24. Bogolyubov E. P., Bochkov V. D., Veretennikov V. A., Vekhoreva L. T., Gribkov V. A., Dubrovskii A. V., Ivanov Y. P., Isakov A. I, Krokhin O. N., Lee P., Lee S., Nikulin V. Y., Serban A., Silin P. V., Feng X., and Zhang G. X. (1998). A powerful soft X-ray source for X-ray lithography based on plasma focusing, *Phys. Scr.*, ***57***, no. 4, pp. 488–494.
25. Siahpoush V., Tafreshi M. A., Sobhanian S., and Khorram S. (2005). Adaptation of Sing Lee's model to the Filippov type plasma focus geometry, *Plasma Phys. Control. Fusion*, ***47***, no. 7, pp. 1065–1075.
26. Lee S. and Saw S. H. (2008). Neutron scaling laws from numerical experiments, *J. Fusion Energy*, ***27***, no. 4, pp. 292–295.
27. Lee S. (2008). Current and neutron scaling for megajoule plasma focus machines, *Plasma Phys. Control. Fusion*, ***50***, no. 10, p. 105 005 (14pp).
28. Lee S., Saw S. H., Lee P. C. K., Rawat R.S., and Schmidt H. (2008). Computing plasma focus pinch current from total current measurement, *Appl. Phys. Lett.* ***92***, no. 11, p. 111 501.
29. Lee S. and Saw S. H. (2008). Pinch current limitation effect in plasma focus, *Appl. Phys. Lett.* ***92***, no. 2, p. 021 503.
30. Lee S., Lee P., Saw S. H., and Rawat R. S. (2008). Numerical experiments on plasma focus pinch current limitation, Plasma Phys. Control. Fusion **50** 065012 (8pp)
31. Web-site: http://www.intimal.edu.my/school/fas/UFLF/ 2010
32. Lee S. (2011). Radiative Dense Plasma Focus Computation Package: RADPF. http://www.plasmafocus.net http://www.plasmafocus.net/IPFS/modelpackage/File1RADPF.htm
33. Saw S. H. and Lee S. (2009). " Scaling laws for plasma focus machines from numerical experiments. IWPDA, Singapore.
34. Lee S. (2009). Diagnostics and Insights from Current waveform and Modelling of Plasma Focus. IWPDA, Singapore.
35. Saw S. H. and Lee S. (2009). Scaling the plasma focus for fusion energy considerations. Tubav Conferences: Nuclear & Renewable Energy Sources, Ankara, Turkey.
36. Lee S. (2009). Neutron Yield Saturation in Plasma Focus-A fundamental cause. *Appl. Phys. Lett.*, 2009, ***95***, 151503 published online.
37. Lee S., Saw S. H., Soto L., Moo S. P., Springham S. V. (2009). Numerical experiments on plasma focus neutron yield versus pressure compared with laboratory experiments, *Plasma Phys. Control. Fusion***, *51*** 075006 (11pp).
38. Lee S., Saw S. H., Lee P. & Rawat R. S. (2009). Numerical Experiments on Neon plasma focus soft x-rays scaling, *Plasma Physics and Controlled Fusion*, ***51***, 105013 (8pp).
39. Akel M., Al-Hawat Sh., Lee S. (2010). Pinch Current and Soft x-ray yield limitation by numerical experiments on Nitrogen Plasma Focus. *J Fusion Energy*. **29**, 94**.**
40. Akel M., Al-Hawat Sh., Lee S.(2009). Numerical Experiments on Soft X-ray Emission Optimization of Nitrogen Plasma in 3 kJ Plasma Focus SY-1 Using Modified Lee Model, *J Fusion Energy* DOI 10.1007/s10894-009-9203-4 First online.
41. M. Akel, Sh. Al-Hawat, S. H. Saw and S. Lee. (2010). Numerical Experiments on Oxygen Soft X-Ray Emissions from Low Energy Plasma Focus Using Lee Model . J Fusion Energy, **29,** 223–231.
42. Lee S., Rawat R. S., Lee P., S H Saw S. H., (2009). Soft x-ray yield from NX2 plasma focus, *J. Appl. Phys*, ***106*****,** 023309.
43. Saw S. H., Lee P. C. K., Rawat R. S. & Lee S. (2009). Optimizing UNU/ICTP PFF Plasma Focus for Neon Soft X-ray Operation. *IEEE Trans on Plasma Sc*, ***37***, 1276-1282.
44. Sing Lee, Sor Heoh Saw. (2010).Numerical Experiments providing new Insights into Plasma Focus Fusion Devices, *Invited Review Paper: Special edition on "Fusion Energy" Energies **3***, 711-737.
45. Lee, S. (2004). *Characterising the Plasma Focus Pinch and Speed Enhancing the Neutron Yield.* In: First Cairo Conf Plasma Physics & Applications. International Cooperation Bilateral Seminars (Vol **34**). Forschungszentrum Juelich GmbH, Juelich, Germany, pp. 27-33. ISBN 3-89336-374-2; 912–919.

46. Chow S. P., Lee S., Tan B. C. (1972) Current sheath studies in a co-axial plasma focus gun .J. of Plasma Phys., **8**: 21-31.
47. Favre M., Lee S., Moo S. P., Wong C. S. (1992). X-ray emission in a small plasma focus operating with H2-Ar mixtures, Plasma Sources Science and Technology, **1** 122-125.
48. Huba J D.(2006). Plasma Formulary page 44 http://wwwppd.nrl.navy.mil/nrlformulary/NRL_FORMULARY_07.pdf
49. Filippov N V, Filippova T I, Khutoretskaia I V, Mialton V V and Vinogradov V P. (1996). Megajoule scale plasma focus as efficient X-ray source, Physics Letters A Vol **211**, Issue 3, 168-171.
50. Rapp H. *Phys Lett A*, (1973), ***43A,*** 420-422.
51. Kraus V. I. (2006). Progress in plasma focus research and applications. 33rd EPS Conference on Plasma Physics, Rome. Plasma Phys. Control. Fusion, **48**, B221-B229.
52. Scholz M. (2007). Report at the ICDMP Meeting, ICDMP, Warsaw, Poland.
53. W Kies. (1988). *Laser and Plasma Technology*, Procs of Second Tropical College Ed by S Lee et al,World Scientific, Singapore ISBN 9971-50-767-6, p86-137.
54. H Herold. (1990). *Laser and Plasma Technology*, Procs of Third Tropical College Ed by C S Wong et al, World Scientific, Singapore ISBN 981-02-0168-0, p21-45.
55. G. Decker, W. Kies, R. Nadolny, P. Rowekamp, F. Schmitz, G. Ziethen, K. N. Koshelev, and Yu. V. Sidelnikov.(1996). Plasma Sources Sci. Technol. **5**, 112.
56. Rishi Verma, P. Lee, S. Lee, S. V. Springham, T. L. Tan, R. S. Rawat, and M. Krishnan. (2008). Order of magnitude enhancement in neutron emission with deuterium-krypton admixture operation in miniature plasma focus device. Appl. Phys. Lett. **93**; doi:10.1063/1.2979683 (*3 pages*).
57. Saw S H. (1991). Experimental studies of a current-stepped pinch. PhD Thesis Universiti Malaya, Malaysia.
58. Lee S. (1984). A current-stepping technique to enhance pinch compression. J *Phys D: Appl Phys* **17**, 733-739.